Research Square

Preprints are preliminary reports that have not undergone peer review.
They should not be considered conclusive, used to inform clinical practice,
or referenced by the media as validated information.

Lumbar Modic Changes Concentrate Stress at the Endplate–Vertebral Interface

Yuchenxi Wang
The First People's Hospital of Yunnan Province, The Affiliated Hospital of Kunming University of Science and Technology

Sunqi Nian
The First People's Hospital of Yunnan Province, The Affiliated Hospital of Kunming University of Science and Technology

Chengjin Li
The First People's Hospital of Yunnan Province, The Affiliated Hospital of Kunming University of Science and Technology

Haotian Luo
The First People's Hospital of Yunnan Province, The Affiliated Hospital of Kunming University of Science and Technology

Guangyao Zhang
The First People's Hospital of Yunnan Province, The Affiliated Hospital of Kunming University of Science and Technology

Fei Chen
The First People's Hospital of Yunnan Province, The Affiliated Hospital of Kunming University of Science and Technology

Na Li
920th Hospital of the Joint Logistics Support Force

Jiayu Chen
jchenspine@163.com

The First People's Hospital of Yunnan Province, The Affiliated Hospital of Kunming University of Science and Technology

---

Research Article

Keywords: Modic changes, finite element analysis, vertebral endplate, disc degeneration, computed tomography, lumbar spine

Posted Date: November 2nd, 2026

DOI: https://doi.org/10.21203/rs.3.rs-11311894/v1

License: This work is licensed under a Creative Commons Attribution 4.0 International License.
Read Full License

Additional Declarations: No competing interests reported.

Lumbar Modic Changes Concentrate Stress at the Endplate–Vertebral Interface

Yuchenxi Wang[a]†, Sunqi Nian[a]†, Chengjin Li[a], Haotian Luo[a], Guangyao Zhang[a], Fei Chen[a], Na Li[b]*, Jiayu Chen[a]*

[a] Department of Orthopaedics, The First People's Hospital of Yunnan Province, The Affiliated Hospital of Kunming University of Science and Technology, Kunming 650500, China.

[b] Department of Anesthesiology, 920th Hospital of Joint Logistic Support Force, Kunming 650032, China.

† Yuchenxi Wang and Sunqi Nian contributed equally to this work.

Corresponding authors

Jiayu Chen, Department of Orthopaedics, The First People's Hospital of Yunnan Province, Kunming 650500, China. Email: jchenspine@163.com. ORCID: 0000-0003-1119-6486.

Na Li, Department of Anesthesiology, 920th Hospital of Joint Logistic Support Force, Kunming 650032, China. Email: lina@kmmu.edu.cn. ORCID: 0000-0003-2821-0547.

Abstract

Background: Modic changes occur where the lumbar disc transfers load to the vertebral body. Regional stress and segmental motion together describe their mechanical effects. We examined how material inputs for each Modic type changed local stress, with and without disc degeneration.

Methods: Paired computed tomography measurements from 24 patients with Modic changes provided stiffness multipliers for each type: seven type I, ten type II, and seven type III cases. Eight L4–L5 finite element models included normal anatomy, isolated disc degeneration, isolated Modic types I–III, and each type combined with disc degeneration. The models shared one base geometry, with a predefined reduction in disc height in degenerated models. Geometry and loading were matched to assess material effects. We applied 500 N compression and a 10 N·m

moment in six directions and descriptively compared endplate and vertebral margin stress, disc stress, and range of motion.

Results: Models containing Modic changes showed focal stress concentration near the mapped region. Isolated Modic changes reduced range of motion by 0.5%–7.7%. Type III had the highest mean margin stress in every tested condition, and maximum stress rankings varied. Maximum L4 margin stress in isolated type III ranged from 13.97 to 36.28 MPa. Geometric mean stiffness multipliers were 2.05, 2.09, and 5.02 for types I, II, and III, respectively. With coexisting disc degeneration, margin stress redistribution depended on vertebral level and loading direction.

Conclusions: In the tested L4–L5 geometry, Modic-related material heterogeneity concentrated stress at the endplate and adjacent vertebral margin. Segmental motion changed relatively little. Local stress assessment complements segmental motion when studying Modic biomechanics.

Keywords: Modic changes; finite element analysis; vertebral endplate; disc degeneration; computed tomography; lumbar spine

Background

Load passes between the lumbar disc and vertebral body through the disc–endplate–bone marrow complex [3–5]. Modic changes (MC) are MRI signal alterations in the adjacent vertebral marrow [1]. Types I, II, and III broadly correspond to inflammatory or edematous, fatty, and sclerotic phenotypes [1,2]. Type I has low T1 and high T2 signal, type II has high signal on both sequences, and type III has low signal on both. These phenotypes place material heterogeneity at an interface where its effect on regional mechanics can be examined.

MC occur in structural and clinical settings where regional load transfer is relevant. They coexist with endplate defects and disc degeneration, and their association with low back pain varies across studies [6–12]. Surgical cohorts have reported associations with recurrent herniation [13,14], fusion outcomes [15–18], and cage subsidence [17,19,20]. Bone quality affects load transfer in lumbar fusion models [21]. Residual symptoms also occur in selected MC cohorts [16–

18,22,23]. These observations provide a clinical context for studying the mechanics of the endplate and adjacent vertebral marrow.

Biological studies also examine this interface. Proposed pathways include endplate microdamage and inflammatory remodeling [3,24–26], bacterial and non-bacterial subgroups [27–32], marrow conversion [3,33,34], and vertebral innervation [35–38]. Experimental endplate injury can induce Modic-like marrow changes [24], and immune cells in affected marrow can degrade cartilage endplates [25]. Regional stress assessment can show how the accompanying material heterogeneity changes load transfer.

Finite element analysis allows comparison of material effects with geometry and loading held constant [39,40]. Earlier lumbar models examined disc degeneration, endplate damage, and segmental motion [41–45]. We used paired computed tomography (CT) Hounsfield unit (HU) measurements to assign material inputs for each Modic type in eight L4–L5 models. Comparisons with and without disc degeneration (DD) assessed endplate and vertebral margin stress together with segmental motion. These matched comparisons identified the regional response to Modic-related material heterogeneity.

Methods

Study design and model groups

We used eight L4–L5 models to compare MC material effects with and without DD. L4–L5 is a common location of lumbar MC [46]. Models included normal anatomy, isolated MC types I–III, isolated DD, and DD combined with each MC type. They shared one base geometry, with a predefined reduction in disc height in DD models. Meshing, contact definitions, boundary conditions, and loading were the same across groups. Material properties varied through the predefined MC and DD modifications.

Patient imaging and MC classification

We retrospectively reviewed lumbar imaging from patients diagnosed with Modic changes between January 2021 and May 2025. Two spine surgeons independently classified blinded MRI examinations as type I, II, or III using established criteria [1,2]. Material calibration included 24 patients: type I, n=7; type II, n=10; and type III, n=7. Eligible patients were older than 18 and younger than 70 years and had MRI-confirmed Modic changes and complete clinical and imaging records. Image quality had to allow segmentation, registration, and HU measurement. We excluded patients with prior spinal surgery, tumor, congenital spinal deformity, metabolic or immune-mediated spinal disease, infectious spinal disease, acute trauma, or incomplete records.

The retrospective imaging review received institutional ethics approval (KHLL2023-KY083), and all participants provided written informed consent. Ethics details are reported in the Declarations section.

MRI examinations used a 1.5-T Siemens system with an eight-channel phased-array spine coil. Classification used sagittal T1-weighted, T2-weighted, and fat-suppressed sequences. Reported spatial parameters were a 200 × 248 matrix, 4.0 mm slice thickness, 0.4 mm interslice gap, and 180 × 300 mm field of view. Agreement before adjudication was Cohen's $\kappa = 0.801$. A third spine specialist resolved three discrepant classifications. Intraclass correlation coefficients, ICC(2,1), were 0.977 for MC-region HU, 0.944 for reference-region HU, and 0.965 for the derived stiffness multiplier (Additional file 1, Figure S1).

Base finite element model

We reconstructed the base L4–L5 model from high-resolution CT of one adult male without known spinal disease. The dataset contained more than 300 contiguous DICOM slices from the upper border of L1 to the sacrum, with a slice thickness of 1.0 mm. We segmented L4 and L5 in Mimics 21.0 using thresholding and manual correction of each slice, then refined the geometry

and reconstructed the disc contours in 3-matic. The model was imported into Ansys 2021 R1 for meshing, material assignment, and solution (Figure 1a).

Mesh characteristics and contact definitions

The global element size was 2 mm, with local refinement to 1 mm in cartilaginous structures. The final L4–L5 mesh contained 148,876 nodes and 525,981 elements.

Facet articular surfaces were frictionless contact pairs. Disc–endplate interfaces were bonded, and ligament attachments were tied to their bony insertion sites. The model did not explicitly include anatomical facet joint clearance.

MRI-CT registration and ROI measurement

We imported MRI and CT datasets into Mimics, identified Modic regions from their MRI signal patterns, and recorded their vertebral level, location adjacent to the endplate, and extent. Vertebral contours, endplate boundaries, and adjacent anatomical landmarks guided matching of the MRI-labeled regions to CT. We checked correspondence on each slice.

After matching MRI and CT, we defined a CT region of interest (ROI) for each Modic region and measured its mean HU. A paired reference ROI was selected at a corresponding cranio-caudal or left–right symmetric location in the same vertebra. Whenever possible, reference ROIs were placed in unaffected marrow, avoiding cortical bone, obvious endplate sclerosis, vascular channels, and artifacts. The dataset contained 41 paired ROIs from 24 patients (Additional file 2, Table S1).

For patient-level HU plots, we separately averaged Modic-region and reference-region measurements across each patient's ROI pairs. We calculated stiffness multipliers for each ROI pair and then averaged them within each patient, as described below. These patient-level multipliers were used for subtype summaries and material assignment.

Anatomic structures and constitutive assumptions

The nonlinear model included cortical and cancellous bone, posterior osseous elements, endplates, the disc, and seven ligamentous structures: the anterior and posterior longitudinal, intertransverse, supraspinous, interspinous, and capsular ligaments, and the ligamentum flavum. Bone and endplates were linear elastic isotropic materials. Nearly incompressible Mooney–Rivlin materials represented the nucleus pulposus and annulus ground substance; the model did not explicitly include annular fiber layers. Ligaments were nonlinear tension-only springs with the properties listed in Table 1.

Ligament moduli, Poisson ratios, and cross-sectional areas were taken from Zhu et al. [47]. Lumbar models of sitting posture and osteoporosis have used similar simplifications for bone and disc materials [48,49].

Construction of MC models

After registering MRI to CT, we mapped the MC region to the right side adjacent to the inferior L4 and superior L5 endplates (Figure 1b and c). Modic models shared this region geometry to isolate the response to material inputs for each type. The asymmetric right-sided region also allowed assessment of stress redistribution with loading direction.

HU-based material assignment

Non-MC cortical and cancellous bone were homogeneous isotropic materials. Cortical bone had an elastic modulus of 12000 MPa and Poisson's ratio of 0.30; the corresponding values for cancellous bone were 100 MPa and 0.25. CT HU measurements provided stiffness multipliers for each MC type. Apparent density and elastic modulus were estimated as $\rho = 47 + 1.122 \times HU$ and $E = 0.63 \times \rho^{1.35}$, respectively [50].

For each paired ROI, we calculated the stiffness multiplier as $k = E(MC) / E(reference)$. The arithmetic mean of ROI-level multipliers gave one value per patient. Subtype estimates were

geometric means of the patient-level values. Two-sided 95% confidence intervals were calculated on the natural-log scale using a t distribution with n − 1 degrees of freedom and then back-transformed to the ratio scale. We also reported medians and interquartile ranges. Each subtype's geometric mean multiplier was used as its finite element material input.

Disc degeneration model

We represented disc degeneration by reducing L4–L5 disc height by 20% and changing the nucleus pulposus Mooney-Rivlin constants (Figure 1d). In the normal model, C10/C01 was 0.12/0.03 MPa for the nucleus pulposus and 0.18/0.045 MPa for the annulus ground substance. In the degenerated model, nucleus pulposus C10/C01 was 0.14/0.035 MPa; annulus ground substance constants remained unchanged. These modifications isolated the effects of disc-height reduction and nucleus dehydration, following previous models of disc degeneration and load redistribution [41–44].

Boundary and loading conditions

We fully constrained the inferior L5 endplate and applied a 500 N axial preload to the superior L4 endplate, followed by a 10 N·m moment in each of six directions: flexion, extension, left and right axial rotation, and left and right lateral bending. All eight models used the same protocol.

Model outputs and analysis

Primary outputs were maximum and mean von Mises stress at the inferior L4 and superior L5 Modic-region margins under each loading condition. Secondary outputs were segmental range of motion (ROM), maximum disc von Mises stress, and endplate and vertebral stress maps. Percentage comparisons used absolute ROM values; signs indicated motion direction.

We extracted segmental ROM and maximum disc von Mises stress under all six loading conditions. Relative changes used prespecified reference models: isolated DD and isolated MC were compared with the normal model, and combined DD plus MC were compared with isolated

DD. ROM relative change was calculated from absolute values as 100 × (|ROM(model)| − |ROM(reference)|) / |ROM(reference)|. Relative change in maximum disc von Mises stress was calculated as 100 × (σ(model) − σ(reference)) / σ(reference), where σ denotes maximum disc von Mises stress.

Each finite element output was a single deterministic solution. We summarized ROM, disc stress, and Modic-region margin stress descriptively.

Baseline ROM comparison

We compared baseline ROM with published in vitro and finite element ranges for comparable loading directions (Figure 2) [51–56]. Agreement supported the model's global motion response under this loading protocol.

Results

Stress concentrated near the mapped MC endplate region

Models containing MC showed focal high-stress regions near the mapped superior endplate region, superimposed on the normal model's peripheral stress band (Figure 3). This pattern was most conspicuous in type III. Isolated DD showed predominantly peripheral stress with local increases along the ring.

Stress also concentrated near the mapped region of the inferior endplate (Figure 4). Normal and isolated DD models had predominantly peripheral stress patterns. In combined models, stress redistribution depended on loading direction, particularly during flexion, lateral bending, and axial rotation.

Type III had the highest mean MC-region margin stress

High-stress bands followed the MC-region margins adjacent to the inferior L4 and superior L5 endplates (Figure 5). Type III had the highest mean margin stress in every tested condition

(Figure 6; Additional file 3). Margin stresses were similar in types I and II. The ranking of maximum stresses varied across conditions.

Across the six directions, maximum L4 margin stress in isolated type III ranged from 13.97 to 36.28 MPa. At L5, isolated models approached 30 MPa in flexion and extension. Combined type III reached 34.34 MPa in extension (Additional file 3, Table S2).

Disc degeneration changed margin stress differently at L4 and L5. In extension, combined models had lower maximum L4 stress and higher maximum L5 stress than isolated Modic models. MC-region margin stress redistribution therefore depended on vertebral level and loading direction.

CT-derived stiffness inputs were higher for type III

Geometric mean MC-to-reference stiffness multipliers were 2.05 (95% confidence interval, 1.82–2.31), 2.09 (1.97–2.22), and 5.02 (3.77–6.68) for types I, II, and III, respectively (Table 2). Estimates for types I and II were similar. Type III had a higher estimate and more variation between patients (Additional file 1, Figure S2). Additional file 2, Table S1 contains the 41 paired ROI measurements.

Local stress concentration accompanied small changes in segmental motion

Isolated MC models had ROM profiles close to normal in all six directions (Figure 7). DD reduced motion more markedly, especially in extension and lateral bending.

Isolated MC reduced ROM by 0.5%–7.7% relative to normal (Table 3; Figure 8a). Flexion values were 2.30°, 2.30°, and 2.29° for types I, II, and III, respectively; normal flexion was 2.48°.

Adding Modic changes to the degenerated-disc model changed ROM by −9.8% to +3.2%, depending on loading direction. Isolated disc degeneration reduced ROM by 17.7%–83.6% relative to normal (Table 3; Figure 8a).

The disc stress response to Modic changes depended on loading direction (Figure 8b; Figure 9; Table 4). Relative to normal, isolated Modic models increased maximum disc von Mises stress by

22.3%–45.5% in flexion, approximately 11.1% in extension, and approximately 14.3% in right axial rotation. Changes were small in left axial rotation. Stress decreased by 6.3%–6.5% in right lateral bending. Adding Modic changes to the degenerated-disc model changed maximum disc stress by −4.4% to +15.9%.

Discussion

Stress concentration at the endplate and adjacent vertebral margin was the main mechanical response to MC-related material heterogeneity. In the matched L4–L5 models, isolated MC caused relatively small changes in ROM. Type III had the highest mean margin stress; peak stress depended on location and loading direction. Stress maps and margin measurements describe a regional response that complements assessment of segmental motion.

Geometry and loading were matched across MC types within each disc condition to compare load transfer across regions of differing assigned stiffness. Earlier lumbar models examined how disc-height loss and nucleus properties affect motion and load sharing [41–44]. Our comparisons extend that approach to material heterogeneity adjacent to the endplate. The regional stress response provides a mechanical context for reported associations among endplate defects, MC, and disc degeneration [4,5,10–12,24,33].

The subtype comparison related the assigned stiffness contrast to margin stress. Types I and II had similar stiffness multipliers and margin stresses, consistent with previous CT observations [57]. The larger type III multiplier accompanied higher mean margin stress. These results describe the response to CT-informed material inputs. Clinical relationships among MC, endplate sclerosis, subsidence, and fusion vary across studies [17,19,20,34,58] and involve bone structure and biology as well as mechanics.

Regional stress assessment added information about MC with coexisting DD. Disc degeneration substantially reduced ROM, while its effects on margin stress depended on vertebral level and

loading direction. Stress and motion describe different aspects of the combined response. The fixed right-sided MC region sets the anatomical context for these directional effects.

The endplate and adjacent vertebral margin are sites where regional mechanics could interact with Modic-associated biological pathways. Modic composition varies within conventional MRI categories [33,59]. Studies describe marrow inflammation, endplate damage, vertebral innervation, and experimental pain behavior [25,26,35,36,38,60–63]. Altered loading at the margin could interact with these processes. Relating regional stress to tissue changes and symptoms would test that link.

In implant studies, the MC-region margin is a candidate site for assessing contact-related load transfer. Reported associations between MC and subsidence or fusion vary across studies [15,17–20]. Models that include endplate integrity, local material properties, and implant geometry could test whether the identified stress pattern affects implant contact mechanics.

The comparisons describe material effects in one L4–L5 geometry with a fixed asymmetric MC region under the specified material assumptions and loading conditions. Endplate and vertebral margin stress measurements characterize the regional response to MC in this setting.

Conclusions

MC-related material heterogeneity concentrated stress at the endplate and adjacent vertebral margin in the tested L4–L5 models. Type III had the highest mean margin stress. Isolated MC caused relatively small changes in ROM, and coexisting DD redistributed margin stress according to vertebral level and loading direction. Regional stress and segmental motion together describe these aspects of Modic biomechanics.

Abbreviations

CI, confidence interval; CT, computed tomography; DD, disc degeneration; DICOM, Digital Imaging and Communications in Medicine; HU, Hounsfield unit; ICC, intraclass correlation

coefficient; IQR, interquartile range; MC, Modic changes; MRI, magnetic resonance imaging; ROI, region of interest; ROM, range of motion.

Declarations

Ethics approval and consent to participate

The retrospective imaging review was approved by the Medical Ethics Committee of the First People's Hospital of Yunnan Province (approval number KHLL2023-KY083; approval date 11 May 2023). Written informed consent was obtained from all participants.

Consent for publication

Written informed consent for publication was obtained from the participants.

Clinical trial number: not applicable.

Availability of data and materials

The reported datasets are included within this article and its additional files. Paired CT HU measurements and derived stiffness multipliers are provided in Additional file 2. MC-region margin stress outputs are provided in Additional file 3. Additional anonymized derived data are available from the corresponding author upon reasonable request and institutional approval. Raw imaging data are not publicly available because of privacy and institutional restrictions.

Competing interests

The authors declare that they have no competing interests.

Funding

This study was supported by the Xingdian Talents Program (XDYC-YLWS-2024-0073); the Yunnan Provincial Science and Technology Department/Kunming Medical University Joint Project of Basic Research (202301AY070001-080); the Reserve Talents for Academic and

Technical Leaders of Middle-aged and Young People in Yunnan Province (202305AC160069); and the Yunnan Provincial Spinal Cord Disease Clinical Medical Centre (No. ZX2022000101).

Authors' contributions

YW performed the investigation and formal analysis and drafted the manuscript. SN contributed to conceptualization and resources and reviewed and edited the manuscript. CL performed the investigation, contributed to supervision, and drafted the manuscript. HL contributed to conceptualization and formal analysis and reviewed and edited the manuscript. GZ contributed to investigation and resources and drafted the manuscript. FC performed formal analysis and reviewed and edited the manuscript. NL contributed to conceptualization and reviewed and edited the manuscript. JC contributed to conceptualization and supervision and drafted the manuscript.

Acknowledgements

We thank the participants whose imaging data contributed to this study.

References

[1] Modic MT, Steinberg PM, Ross JS, Masaryk TJ, Carter JR. Degenerative disk disease: assessment of changes in vertebral body marrow with MR imaging. Radiology. 1988;166(1 Pt 1):193-199. doi:10.1148/radiology.166.1.3336678.

[2] Fields AJ, Battie MC, Herzog RJ, Jarvik JG, Krug R, Link TM, et al. Measuring and reporting of vertebral endplate bone marrow lesions as seen on MRI (Modic changes): recommendations from the ISSLS Degenerative Spinal Phenotypes Group. Eur Spine J. 2019;28(10):2266-2274. doi:10.1007/s00586-019-06119-6.

[3] Dudli S, Fields AJ, Samartzis D, Karppinen J, Lotz JC. Pathobiology of Modic changes. Eur Spine J. 2016;25(11):3723-3734. doi:10.1007/s00586-016-4459-7.

[4] Rajasekaran S, Bt P, Murugan C, Mengesha MG, Easwaran M, Naik AS, et al. The disc-endplate-bone-marrow complex classification: progress in our understanding of Modic vertebral endplate changes and their clinical relevance. Spine J. 2024;24(1):34-45. doi:10.1016/j.spinee.2023.09.002.

[5] Rajasekaran S, Ramachandran K, K S SVA, Kanna RM, Shetty AP. From Modic to disc endplate bone marrow complex: the natural course and clinical implication of vertebral endplate changes. Global Spine J. 2025;15(1):196-209. doi:10.1177/21925682241271440.

[6] Kjaer P, Korsholm L, Bendix T, Sorensen JS, Leboeuf-Yde C. Modic changes and their associations with clinical findings. Eur Spine J. 2006;15(9):1312-1319. doi:10.1007/s00586-006-0185-x.

[7] Jensen TS, Karppinen J, Sorensen JS, Niinimaki J, Leboeuf-Yde C. Vertebral endplate signal changes (Modic change): a systematic literature review of prevalence and association with non-specific low back pain. Eur Spine J. 2008;17(11):1407-1422. doi:10.1007/s00586-008-0770-2.

[8] Herlin C, Kjaer P, Espeland A, Skouen JS, Leboeuf-Yde C, Karppinen J, et al. Modic changes: their associations with low back pain and activity limitation: a systematic literature review and meta-analysis. PLoS One. 2018;13(8):e0200677. doi:10.1371/journal.pone.0200677.

[9] Hopayian K, Raslan E, Soliman S. The association of Modic changes and chronic low back pain: a systematic review. J Orthop. 2023;35:99-106. doi:10.1016/j.jor.2022.11.003.

[10] Maatta JH, Rade M, Freidin MB, Airaksinen O, Karppinen J, Williams FMK. Strong association between vertebral endplate defect and Modic change in the general population. Sci Rep. 2018;8(1):16630. doi:10.1038/s41598-018-34933-3.

[11] Rade M, Maatta JH, Freidin MB, Airaksinen O, Karppinen J, Williams FMK. Vertebral endplate defect as initiating factor in intervertebral disc degeneration: strong association between endplate defect and disc degeneration in the general population. Spine (Phila Pa 1976). 2018;43(6):412-419. doi:10.1097/BRS.0000000000002352.

[12] Mok FPS, Samartzis D, Karppinen J, Fong DYT, Luk KDK, Cheung KMC. Modic changes of the lumbar spine: prevalence, risk factors, and association with disc degeneration and low back pain in a large-scale population-based cohort. Spine J. 2016;16(1):32-41. doi:10.1016/j.spinee.2015.09.060.

[13] Li X, Ren H, Peng L, Yuan J. Association between Modic changes and recurrence of lumbar disc herniation after percutaneous endoscopic lumbar discectomy: a meta-analysis. Front Surg. 2025;12:1694557. doi:10.3389/fsurg.2025.1694557.

[14] Hao L, Li S, Liu J, Shan Z, Fan S, Zhao F. Recurrent disc herniation following percutaneous endoscopic lumbar discectomy preferentially occurs when Modic changes are present. J Orthop Surg Res. 2020;15(1):176. doi:10.1186/s13018-020-01695-6.

[15] Chen R, Zou K, Liu J, Li K, Zhou Y, Huang H, et al. Do Modic changes affect the fusion rate in spinal interbody fusion surgery? A systematic review and network meta-analysis. J Clin Neurosci. 2024;125:110-119. doi:10.1016/j.jocn.2024.05.019.

[16] Xiao Y, Xiu P, Yang X, Wang L, Li T, Gong Q, et al. Does preoperative Modic changes influence the short-term fusion rate of single level transforaminal lumbar interbody fusion? A matched-pair case control study. Orthop Surg. 2023;15(9):2309-2317. doi:10.1111/os.13795.

[17] Zhang X, Qiao X, Zhou X, Wang L. A new Modic changes classification and its impact on posterior lumbar interbody fusion. BMC Musculoskelet Disord. 2025;26(1):1110. doi:10.1186/s12891-025-09332-1.

[18] Xiao Y, Zhu C, Xiu P, Wang L, Zhang Z, Deng Z, et al. Postoperative sclerotic Modic changes after transforaminal lumbar interbody fusion: the prevalence, risk factors, and impact on fusion. Spine (Phila Pa 1976). 2024;49(10):E135-E141. doi:10.1097/BRS.0000000000004890.

[19] Duan Y, Feng D, Zhu M, Qiu H, Li T, Chen Z, et al. Modic changes increase the cage subsidence rate in spinal interbody fusion surgery: a systematic review and network meta-analysis. World Neurosurg. 2024;181:64-72. doi:10.1016/j.wneu.2023.10.080.

[20] Liu J, Ding W, Yang D, Wu H, Hao L, Hu Z, et al. Modic changes associated with endplate sclerosis can prevent cage subsidence in oblique lumbar interbody fusion stand-alone. World Neurosurg. 2020;138:e160-e168. doi:10.1016/j.wneu.2020.02.047.

[21] Liu C, Zhao M, Zhang W, Wang C, Hu B, Wang K, et al. Biomechanical assessment of different transforaminal lumbar interbody fusion constructs in normal and osteoporotic condition: a finite element analysis. Spine J. 2024;24(6):1121-31. doi:10.1016/j.spinee.2024.01.017.

[22] Albert HB, Manniche C. Modic changes following lumbar disc herniation. Eur Spine J. 2007;16(7):977-982. doi:10.1007/s00586-007-0336-8.

[23] Nian S, Li N, Kong F, Lu S, Chen J. Is discectomy effective for treating low back pain in patients with lumbar disc herniation and Modic changes? A systematic review and meta-analysis of cohort studies. Spine J. 2023;23(4):533-549. doi:10.1016/j.spinee.2022.10.008.

[24] Wang D, Lai A, Gansau J, Seifert AC, Munitz J, Zaheer K, et al. Lumbar endplate microfracture injury induces Modic-like changes, intervertebral disc degeneration and spinal cord sensitization: an in vivo rat model. Spine J. 2023;23(9):1375-1388. doi:10.1016/j.spinee.2023.04.012.

[25] Heggli I, Mengis T, Devan J, Herger N, Farshad M, Habib M, et al. Modic change bone marrow neutrophils are activated and degrade cartilage endplates. JOR Spine. 2026;9(1):e70170. doi:10.1002/jsp2.70170.

[26] Chen H, Zhou Q, Pu X, Wang N, Wang S, Feng Z, et al. Association between vertebral endplate defects and patient-reported symptoms: an immunohistochemical study investigating the COX-2/PGE-2/EP-4 axis. Spine J. 2024;24(8):1407-1415. doi:10.1016/j.spinee.2024.04.003.

[27] Gilligan CJ, Cohen SP, Fischetti VA, Hirsch JA, Czaplewski LG. Chronic low back pain, bacterial infection and treatment with antibiotics. Spine J. 2021;21(6):903-914. doi:10.1016/j.spinee.2021.02.009.

[28] Urquhart DM, Zheng Y, Cheng AC, Rosenfeld JV, Chan P, Liew S, et al. Could low grade bacterial infection contribute to low back pain? A systematic review. BMC Med. 2015;13:13. doi:10.1186/s12916-015-0267-x.

[29] Albert HB, Sorensen JS, Christensen BS, Manniche C. Antibiotic treatment in patients with chronic low back pain and vertebral bone edema (Modic type 1 changes): a double-blind randomized clinical controlled trial of efficacy. Eur Spine J. 2013;22(4):697-707. doi:10.1007/s00586-013-2675-y.

[30] Bråten LCH, Rolfsen MP, Espeland A, Wigemyr M, Aßmus J, Froholdt A, et al. Efficacy of antibiotic treatment in patients with chronic low back pain and Modic changes (the AIM study): double blind, randomised, placebo controlled, multicentre trial. BMJ. 2019;367:l5654. doi:10.1136/bmj.l5654.

[31] Heggli I, Mengis T, Laux CJ, Opitz L, Herger N, Menghini D, et al. Low back pain patients with Modic type 1 changes exhibit distinct bacterial and non-bacterial subtypes. Osteoarthritis Cartilage Open. 2024;6(1):100434. doi:10.1016/j.ocarto.2024.100434.

[32] Nian S, Tang S, Shen S, Yue W, Zhao C, Zou T, et al. Landscape of the lumbar cartilaginous end plate microbiota and metabolites in patients with Modic changes. J Bone Joint Surg Am. 2024;106(20):1866-1875. doi:10.2106/JBJS.23.00805.

[33] Bonnheim NB, Brumm Z, Link TM, Akkaya Z, Lazar AA, Lotz JC, et al. Vertebral endplate bone marrow lesion composition: relation to Modic change classification and associations with chronic low back pain. Spine J. 2026. doi:10.1016/j.spinee.2026.05.002.

[34] Perilli E, Parkinson IH, Truong LH, Chong KC, Fazzalari NL, Osti OL. Modic (endplate) changes in the lumbar spine: bone micro-architecture and remodelling. Eur Spine J. 2015;24(9):1926-1934. doi:10.1007/s00586-014-3455-z.

[35] Fras C, Kravetz P, Mody DR, Heggeness MH. Substance P-containing nerves within the human vertebral body: an immunohistochemical study of the basivertebral nerve. Spine J. 2003;3(1):63-67. doi:10.1016/s1529-9430(02)00455-2.

[36] Bailey JF, Liebenberg E, Degmetich S, Lotz JC. Innervation patterns of PGP 9.5-positive nerve fibers within the human lumbar vertebra. J Anat. 2011;218(3):263-270. doi:10.1111/j.1469-7580.2010.01332.x.

[37] Ehsanian R, Buttner JA, Schneider B, McCormick ZL. Patient selection, clinical outcomes, associated healthcare utilization, and cost-effectiveness of basivertebral nerve ablation for the treatment of vertebrogenic low back pain: a narrative review. N Am Spine Soc J. 2025;24:100788. doi:10.1016/j.xnsj.2025.100788.

[38] Wen J, Kou M, Abed I, Park D, Muttalib Z, Alam A, et al. Modic changes and their role in vertebrogenic back pain: a literature review. Skeletal Radiol. 2026;55(2):249-261. doi:10.1007/s00256-025-05065-3.

[39] Sun T, Wang J, Liu X, Huang H, Wang J, Suo M, et al. Finite element models of intervertebral disc: recent advances and prospects. Ann Med. 2025;57(1):2453089. doi:10.1080/07853890.2025.2453089.

[40] Hani H, Knapik GG, Bourekas EC, Marras WS. Biomechanical models of lumbar spine degeneration: methods, challenges, and clinical promise. Clin Biomech (Bristol). 2025;130:106675. doi:10.1016/j.clinbiomech.2025.106675.

[41] Bashkuev M, Reitmaier S, Schmidt H. Effect of disc degeneration on the mechanical behavior of the human lumbar spine: a probabilistic finite element study. Spine J. 2018;18(10):1910-1920. doi:10.1016/j.spinee.2018.05.046.

[42] Cai XY, Sun MS, Huang YP, Liu ZX, Liu CJ, Du CF, et al. Biomechanical effect of L4-L5 intervertebral disc degeneration on the lower lumbar spine: a finite element study. Orthop Surg. 2020;12(3):917-930. doi:10.1111/os.12703.

[43] Galbusera F, Schmidt H, Neidlinger-Wilke C, Gottschalk A, Wilke HJ. The mechanical response of the lumbar spine to different combinations of disc degenerative changes investigated using randomized poroelastic finite element models. Eur Spine J. 2011;20(4):563-571. doi:10.1007/s00586-010-1586-4.

[44] Park WM, Kim K, Kim YH. Effects of degenerated intervertebral discs on intersegmental rotations, intradiscal pressures, and facet joint forces of the whole lumbar spine. Comput Biol Med. 2013;43(9):1234-1240. doi:10.1016/j.compbiomed.2013.06.011.

[45] Rajasekaran S, Jebaseelan D, Gurusamy G, Devaraj KB, Harinathan B, Yoganandan N. Minor endplate damage as an initiator of systemic biomechanical disruption of the lumbar disc: a finite element analysis of the mechanical tipping point in disc failure. Eur Spine J. 2026;35:3809–3821. doi:10.1007/s00586-026-09983-1.

[46] Huang ZY, Xu HC, Lei T, Li QL, Wu AM, Ni WF. The location of Modic changes in the lumbar spine: a meta-analysis. Eur Spine J. 2016;25(11):3746-3759. doi:10.1007/s00586-016-4456-x.

[47] Zhu T, Xu Z, Liu D, Zeng W, Pu Y, Yang H. Biomechanical influence of numerical variants of lumbosacral transitional vertebra with Castellvi type I on adjacent discs and facet joints based on 3D finite element analysis. Bone Rep. 2025;24:101831. doi:10.1016/j.bonr.2025.101831.

[48] Cho M, Han JS, Kang S, Ahn CH, Kim DH, Kim CH, et al. Biomechanical effects of different sitting postures and physiologic movements on the lumbar spine: a finite element study. Bioengineering (Basel). 2023;10(9):1051. doi:10.3390/bioengineering10091051.

[49] Kang S, Park CH, Jung H, Lee S, Min YS, Kim CH, et al. Analysis of the physiological load on lumbar vertebrae in patients with osteoporosis: a finite-element study. Sci Rep. 2022;12(1):11001. doi:10.1038/s41598-022-15241-3.

[50] Rho JY, Hobatho MC, Ashman RB. Relations of mechanical properties to density and CT numbers in human bone. Med Eng Phys. 1995;17(5):347-355. doi:10.1016/1350-4533(95)97314-f.

[51] Gonzalez Gutierrez RA, Rangel Alonso V, Barraza Armenta CM. Flexibility of the lumbar intervertebral disc in bending and torsion: experimental and finite element study. Journal of Mechanics Engineering and Automation. 2017;7(4):203-208. doi:10.17265/2159-5275/2017.04.004.

[52] Yamamoto I, Panjabi MM, Crisco T, Oxland T. Three-dimensional movements of the whole lumbar spine and lumbosacral joint. Spine (Phila Pa 1976). 1989;14(11):1256-1260. doi:10.1097/00007632-198911000-00020.

[53] Han Z, Ma C, Li B, Ren B, Liu J, Huang Y, et al. Biomechanical studies of different numbers and positions of cage implantation on minimally invasive transforaminal interbody fusion: a finite element analysis. Front Surg. 2022;9:1011808. doi:10.3389/fsurg.2022.1011808.

[54] Masni-Azian A, Tanaka M. Biomechanical investigation on the influence of the regional material degeneration of an intervertebral disc in a lower lumbar spinal unit: a finite element study. Comput Biol Med. 2018;98:26-38. doi:10.1016/j.compbiomed.2018.05.010.

[55] Lv QB, Gao X, Pan XX, Jin HM, Lou XT, Li SM, et al. Biomechanical properties of novel transpedicular transdiscal screw fixation with interbody arthrodesis technique in lumbar spine: a finite element study. J Orthop Transl. 2018;15:50-58. doi:10.1016/j.jot.2018.08.005.

[56] Sengul E, Ozmen R, Demir T. The biomechanical performance investigation of L4-L5 lumbar segment by finite element method. In: Proceedings of the 6th World Congress on Electrical Engineering and Computer Systems and Science; Virtual Conference; August 2020. Paper No. ICBES 103. doi:10.11159/icbes20.103.

[57] Kuisma M, Karppinen J, Haapea M, Lammentausta E, Niinimaki J, Tervonen O. Modic changes in vertebral endplates: a comparison of MR imaging and multislice CT. Skeletal Radiol. 2009;38(2):141-147. doi:10.1007/s00256-008-0590-9.

[58] Duan Y, Feng D, Zou K, Yang F, Chen R, Huang Y. The relationship between Modic changes and endplate sclerosis in patients with lumbar degenerative disease: a systematic review and network meta-analysis. World Neurosurg. 2024;186:7-16. doi:10.1016/j.wneu.2024.03.017.

[59] Nian S, Li C, Chen F, Zhao C, Zhang G, Li N, et al. MRI radiomics reveals pain-related biomarkers for Modic changes. Eur Spine J. 2026;35(3):1194-1203. doi:10.1007/s00586-025-09592-4.

[60] Ni S, Ling Z, Wang X, Cao Y, Wu T, Deng R, et al. Sensory innervation in porous endplates by Netrin-1 from osteoclasts mediates PGE2-induced spinal hypersensitivity in mice. Nat Commun. 2019;10(1):5643. doi:10.1038/s41467-019-13476-9.

[61] Xue P, Wang S, Lyu X, Wan M, Li X, Ma L, et al. PGE2/EP4 skeleton interoception activity reduces vertebral endplate porosity and spinal pain with low-dose celecoxib. Bone Res. 2021;9(1):36. doi:10.1038/s41413-021-00155-z.

[62] Ling Z, Crane J, Hu H, Chen Y, Wan M, Ni S, et al. Parathyroid hormone treatment partially reverses endplate remodeling and attenuates low back pain in animal models of spine degeneration. Sci Transl Med. 2023;15(722):eadg8982. doi:10.1126/scitranslmed.adg8982.

[63] Pan D, Benkato KG, Han X, Zheng J, Kumar V, Wan M, et al. Senescence of endplate osteoclasts induces sensory innervation and spinal pain. eLife. 2024;12:e92889. doi:10.7554/eLife.92889.

Figure legends

Figure 1. L4–L5 finite element models constructed in Ansys Workbench 2021 R1. (a) Normal control. (b) Modic change. (c) Disc degeneration combined with Modic change. (d) Disc degeneration.

Figure 2. Baseline segmental motion comparison. Range of motion (ROM) was compared with published in vitro and finite element data under six loading conditions.

Figure 3. Superior endplate von Mises stress maps under six loading conditions. Rows a–h show normal, isolated disc degeneration, isolated Modic types I, II, and III, and disc degeneration combined with Modic types I, II, and III, respectively. MC, Modic changes.

Figure 4. Inferior endplate von Mises stress maps under six loading conditions. Rows a–h show normal, isolated disc degeneration, isolated Modic types I, II, and III, and disc degeneration combined with Modic types I, II, and III, respectively. MC, Modic changes.

Figure 5. Vertebral von Mises stress maps under six loading conditions. Rows a–h show normal, isolated disc degeneration, isolated Modic types I, II, and III, and disc degeneration combined with Modic types I, II, and III, respectively. Modic regions are located on the right side adjacent to the inferior L4 and superior L5 endplates. MC, Modic changes.

Figure 6. Modic-region margin stress in isolated and combined models. (a, b) Maximum and mean L4 margin stress. (c, d) Maximum and mean L5 margin stress. The horizontal axis shows the six loading conditions. Colors indicate types I–III; solid lines show isolated Modic models and dashed lines show combined models. Small horizontal offsets separate overlapping type I and II traces without changing stress values. Values are deterministic outputs in MPa. Normal and isolated disc-degeneration models have no defined Modic-region margin and are not shown. DD, disc degeneration; MC, Modic changes.

Figure 7. ROM profiles under six loading conditions. Panels a–g compare the normal model (black) with isolated disc degeneration, isolated Modic types I, II, and III, and disc degeneration

combined with each type, respectively. Radial values are absolute ROM in degrees; extension, right axial rotation, and right lateral bending are displayed as magnitudes. DD, disc degeneration; MC, Modic changes; ROM, range of motion.

Figure 8. Relative changes in segmental motion and maximum disc stress. (a) Segmental ROM; (b) maximum disc von Mises stress. For isolated disc degeneration and isolated MC models, values are expressed relative to the normal model. For combined disc degeneration plus MC models, values are expressed relative to the isolated disc degeneration model. ROM changes were calculated from absolute values as $100 \times (|\mathrm{ROM(model)}| - |\mathrm{ROM(reference)}|) / |\mathrm{ROM(reference)}|$; maximum disc von Mises stress changes were calculated as $100 \times (\sigma(\mathrm{model}) - \sigma(\mathrm{reference})) / \sigma(\mathrm{reference})$, where σ denotes maximum disc von Mises stress. Blue indicates a relative reduction, red indicates a relative increase, and white indicates no relative change. Each cell represents one deterministic finite element solution and does not represent statistical significance. DD, disc degeneration; MC, Modic changes.

Figure 9. L4–L5 disc von Mises stress maps under six loading conditions. Rows a–h show normal, isolated disc degeneration, isolated Modic types I, II, and III, and disc degeneration combined with Modic types I, II, and III, respectively. Columns show flexion, extension, left and right axial rotation, and left and right lateral bending. MC, Modic changes.

Tables

Table 1. Ligament material parameters and source.

Ligament	Elastic Modulus (MPa)	Poisson's Ratio	Cross-sectional Area (mm²)	Direct source
Anterior longitudinal ligament	20	0.30	63.7	[47]
Posterior longitudinal ligament	20	0.30	20	[47]
Intertransverse ligament	58.7	0.30	3.6	[47]

Ligament	Elastic Modulus (MPa)	Poisson's Ratio	Cross-sectional Area (mm²)	Direct source
Supraspinous ligament	15	0.30	30	[47]
Interspinous ligament	11.6	0.30	40	[47]
Capsular ligament	32.9	0.30	60	[47]
Ligamentum flavum	19.5	0.30	40	[47]

Source: Ligament material properties were adopted from Zhu et al. [47].

Table 2. Patient-level HU-derived stiffness multipliers by Modic change type.

Type	n	GM (ratio)	Median (ratio)	Q1 (ratio)	Q3 (ratio)	IQR (ratio)	Geometric mean, 95% CI (ratio)
I	7	2.05	2.02	1.86	2.22	0.36	1.82–2.31
II	10	2.09	2.06	1.96	2.22	0.26	1.97–2.22
III	7	5.02	4.39	4.03	6.42	2.39	3.77–6.68

GM, geometric mean; CI, confidence interval; IQR, interquartile range. The 95% confidence intervals were calculated on the natural-log scale using the t distribution with (n − 1) degrees of freedom and back-transformed to the original ratio scale. Values are patient-level stiffness multipliers relative to paired reference regions.

Table 3. Segmental range of motion under compression and moments.

Model	Flexion	Extension	Left axial rotation	Right axial rotation	Left lateral bending	Right lateral bending
Normal	2.48	-3.84	5.29	-5.07	5.26	-4.52
Disc degeneration	2.04	-0.63	3.14	-2.82	1.61	-0.98
MC I	2.30	-3.82	5.04	-4.97	5.06	-4.26

Model	Flexion	Extension	Left axial rotation	Right axial rotation	Left lateral bending	Right lateral bending
MC II	2.30	-3.82	5.04	-4.97	5.05	-4.25
MC III	2.29	-3.81	5.04	-4.97	5.04	-4.25
Disc degeneration + MC I	1.85	-0.65	3.00	-2.76	1.57	-0.96
Disc degeneration + MC II	1.85	-0.65	3.00	-2.76	1.57	-0.96
Disc degeneration + MC III	1.84	-0.65	3.00	-2.76	1.57	-0.95

542 ROM values are in degrees. Negative signs indicate motion direction only; percentage changes were calculated using
543 absolute values.

Table 4. Maximum von Mises stress in the L4-L5 disc.

Model	Flexion	Extension	Left rotation	Right rotation	Left bending	Right bending
Normal	1.21	2.08	2.17	1.82	4.16	4.92
Disc degeneration	0.90	0.64	2.05	2.54	1.35	1.32
MC I	1.76	2.31	2.17	2.08	4.45	4.61
MC II	1.73	2.31	2.17	2.08	4.45	4.61
MC III	1.48	2.31	2.17	2.08	4.45	4.60
Disc degeneration + MC I	0.86	0.72	1.98	2.49	1.45	1.53
Disc degeneration + MC II	0.86	0.72	1.98	2.49	1.44	1.53
Disc degeneration + MC III	0.86	0.72	1.98	2.49	1.44	1.52

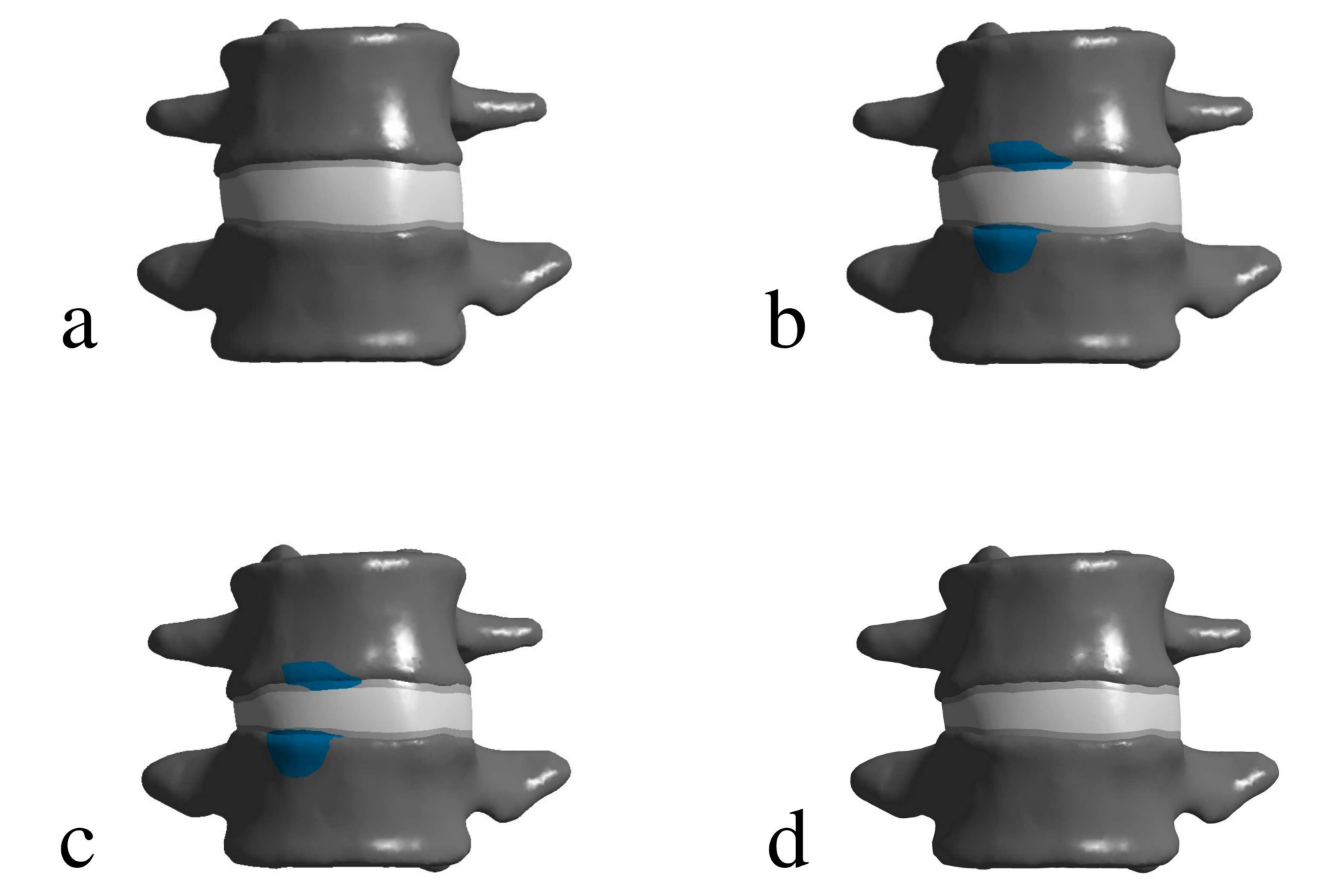
544 Stress values are MPa.

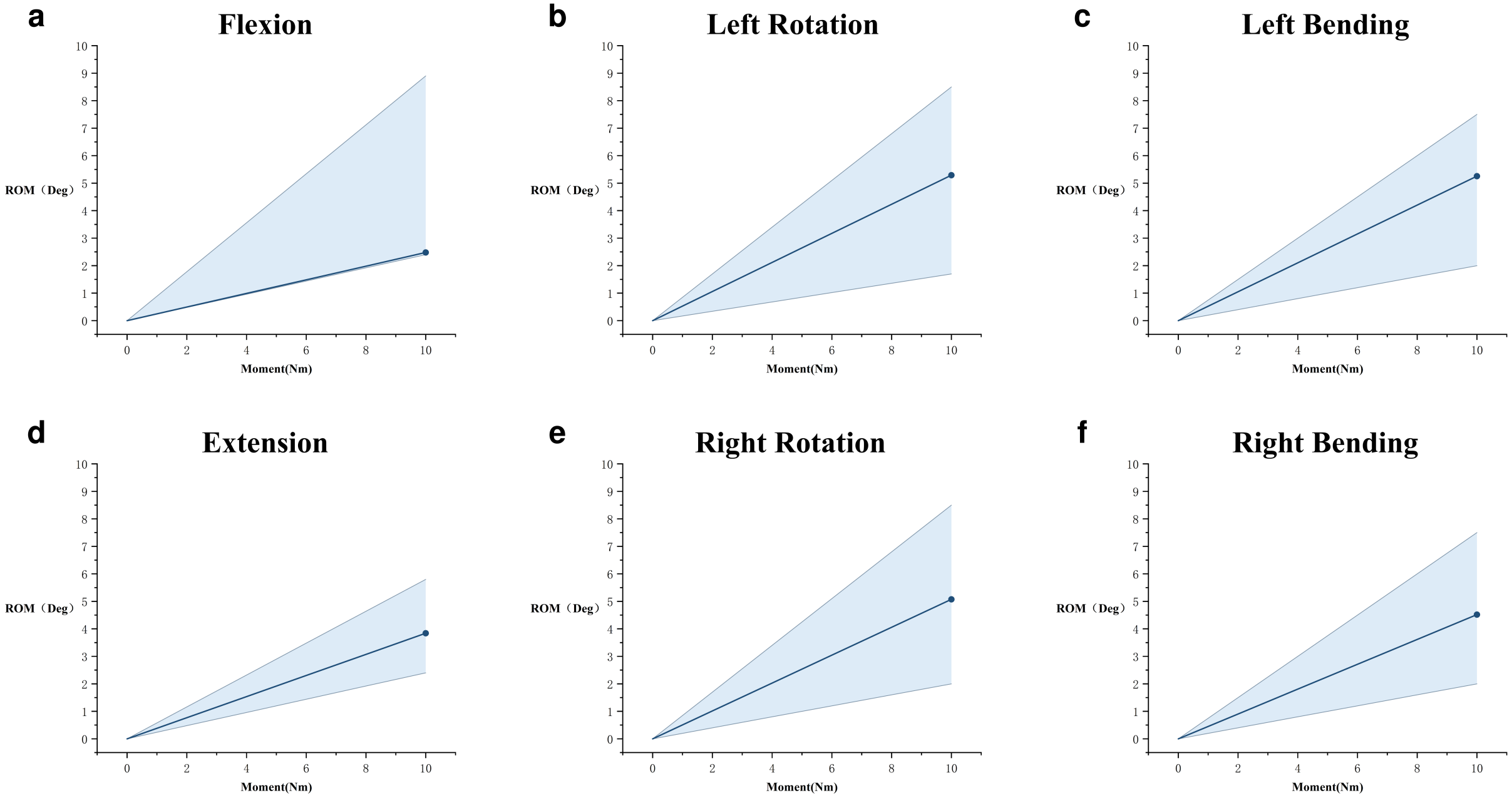
Additional files

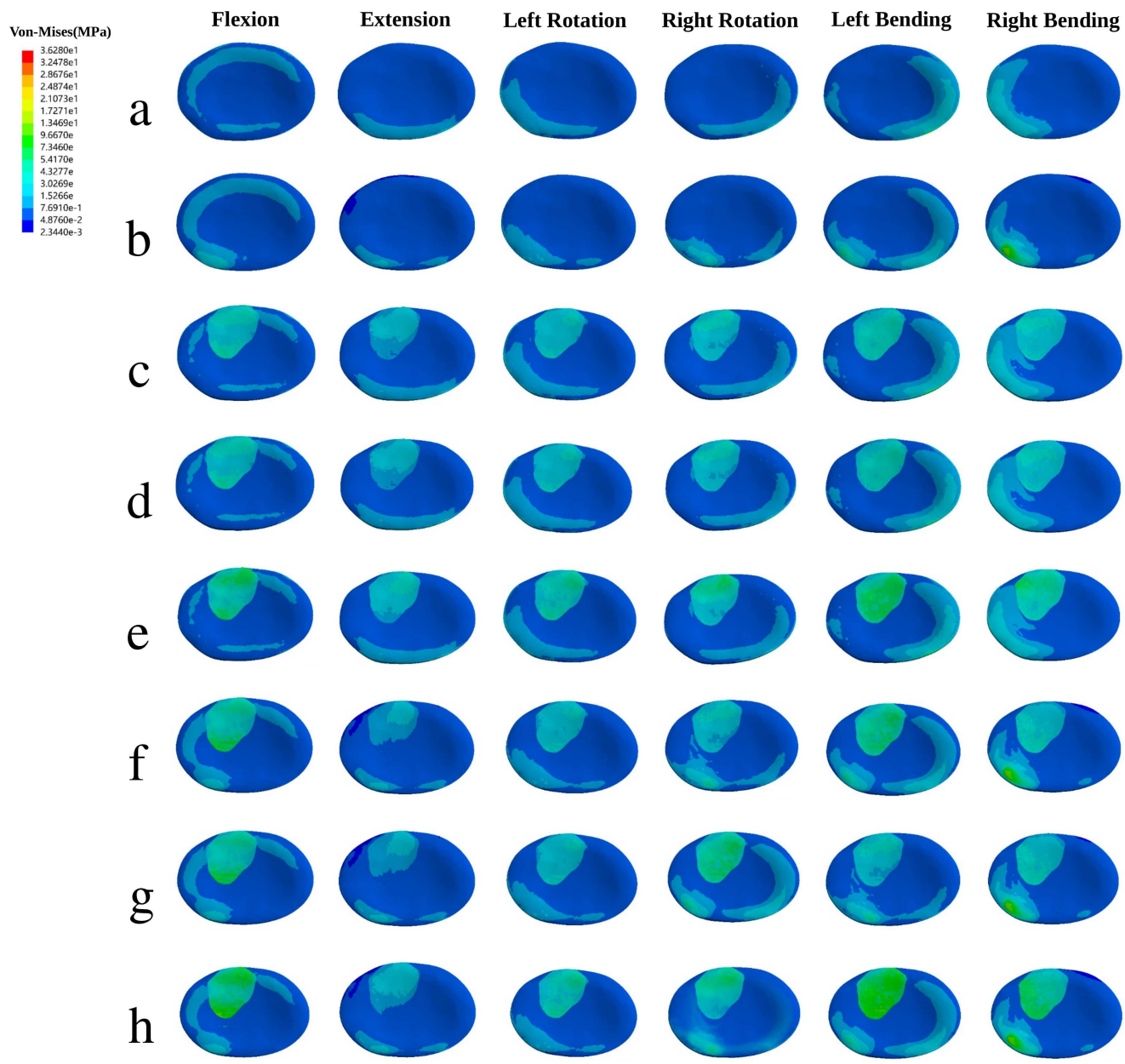
Additional file 1: Additional_file_1.docx. Supplementary figures S1 and S2 showing repeatability of HU-derived inputs and patient-level HU measurements and stiffness multipliers.

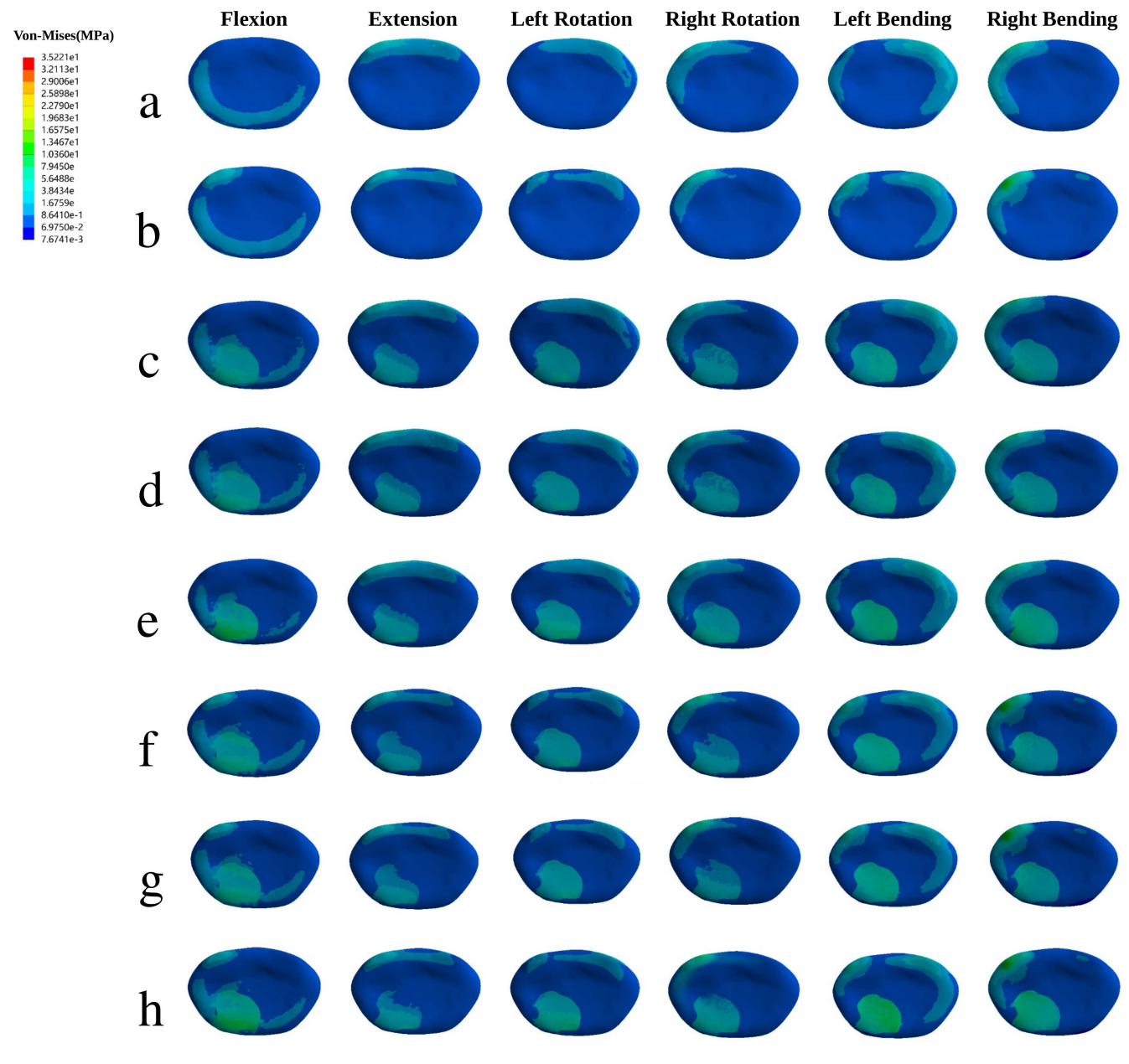
Additional file 2: Additional_file_2.csv. Supplementary Table S1 containing 41 paired ROI measurements from 24 patients and derived stiffness multipliers.

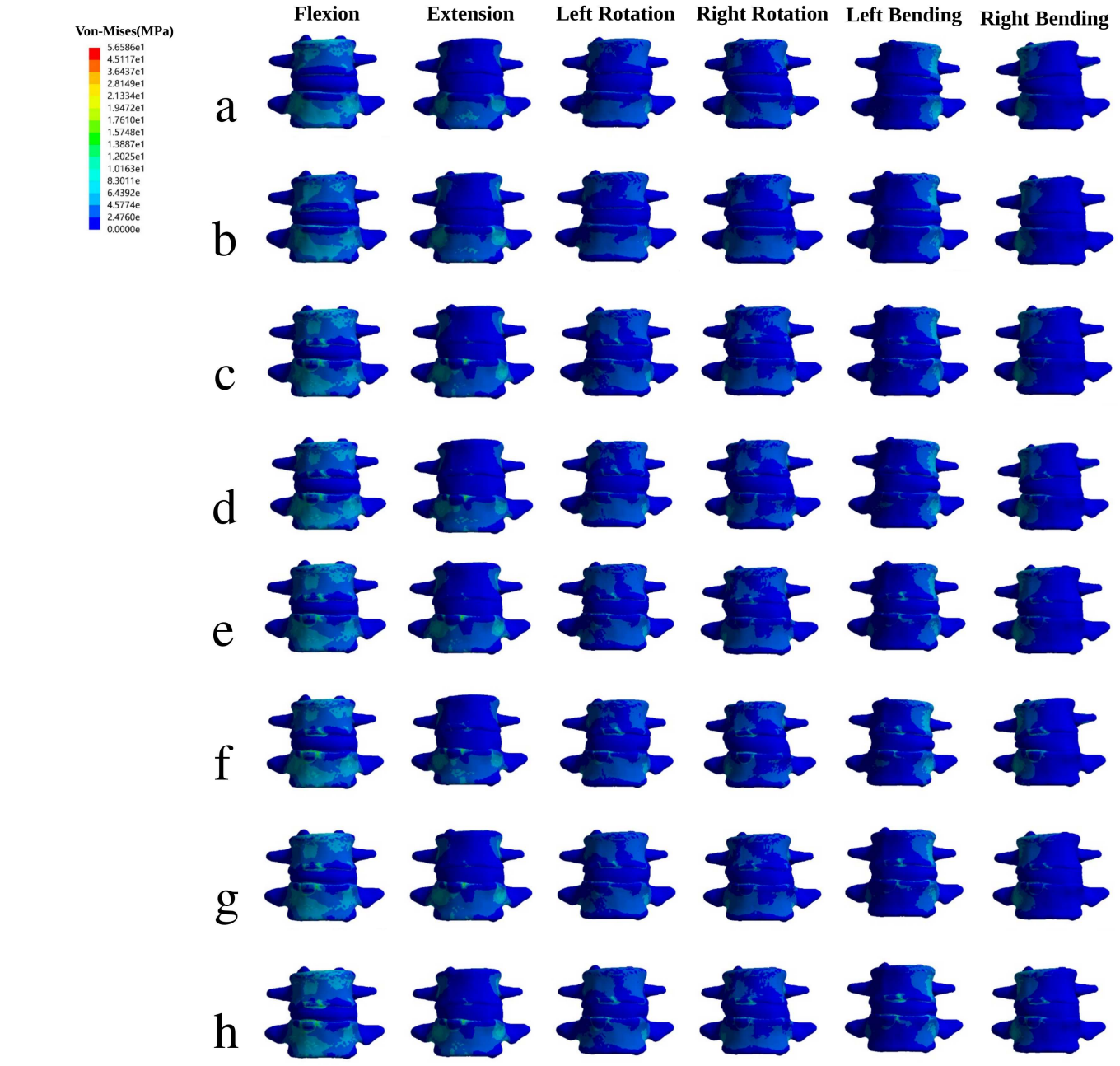
Additional file 3: Additional_file_3.csv. Supplementary Table S2 containing maximum and mean MC-region margin stresses under six loading conditions.

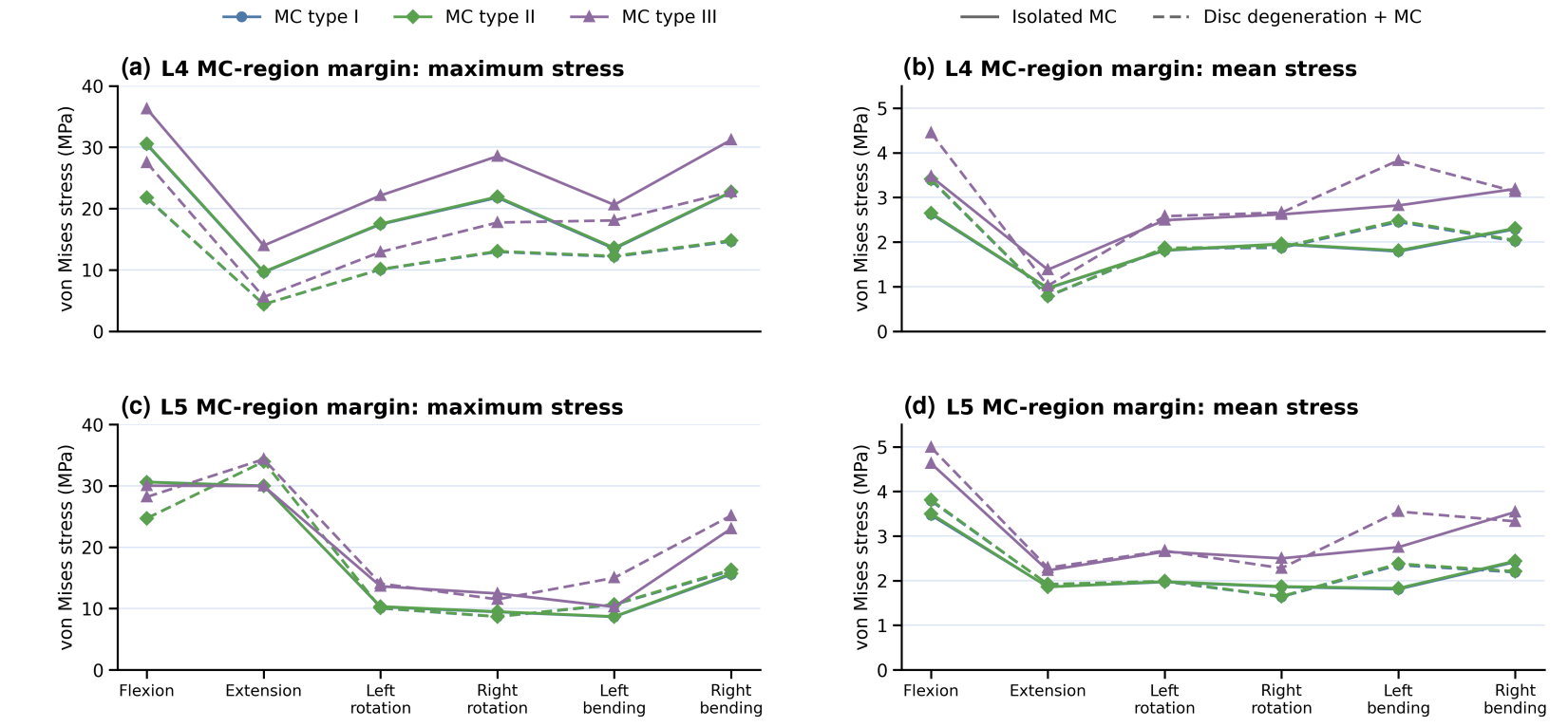

a
b
c
d

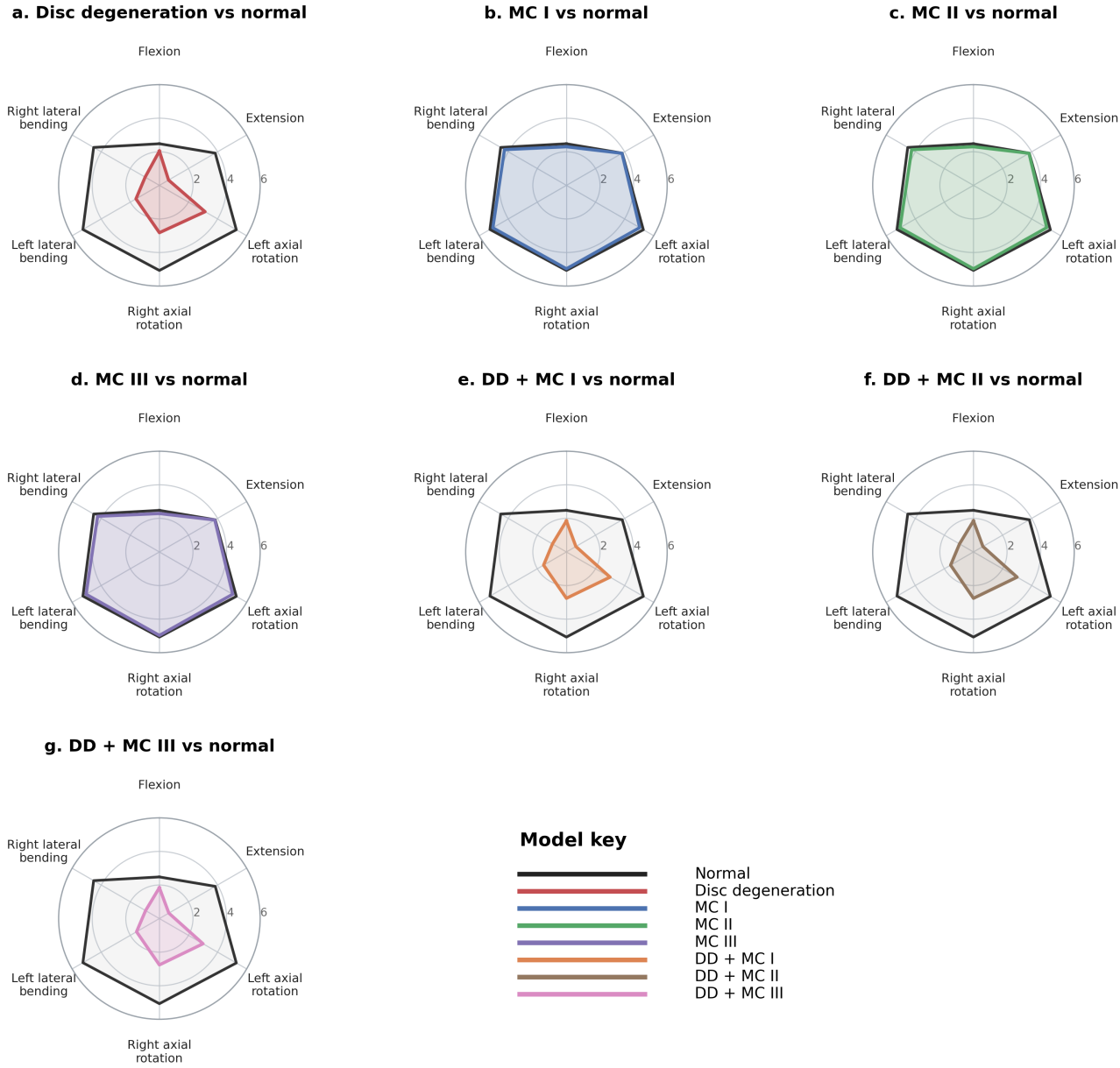

a
Flexion
b
Left Rotation
c
Left Bending
d
Extension
e
Right Rotation
f
Right Bending
ROM（Deg）
Moment(Nm)
0
1
2
3
4
5
6
7
8
9
10

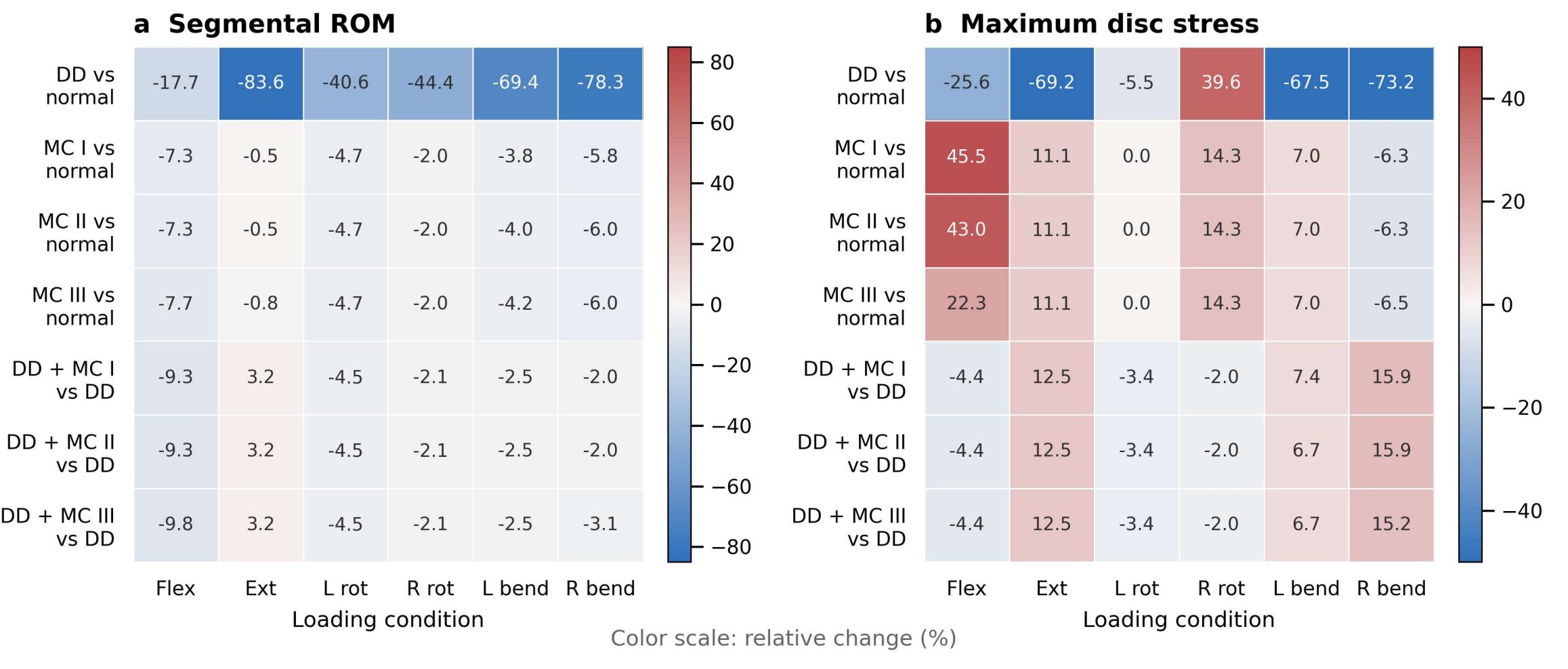

Von-Mises(MPa)
3.6280e1
3.2478e1
2.8676e1
2.4874e1
2.1073e1
1.7271e1
1.3469e1
9.6670e
7.3460e
5.4170e
4.3277e
3.0269e
1.5266e
7.6910e-1
4.8760e-2
2.3440e-3
Flexion
Extension
Left Rotation
Right Rotation
Left Bending
Right Bending
a
b
c
d
e
f
g
h

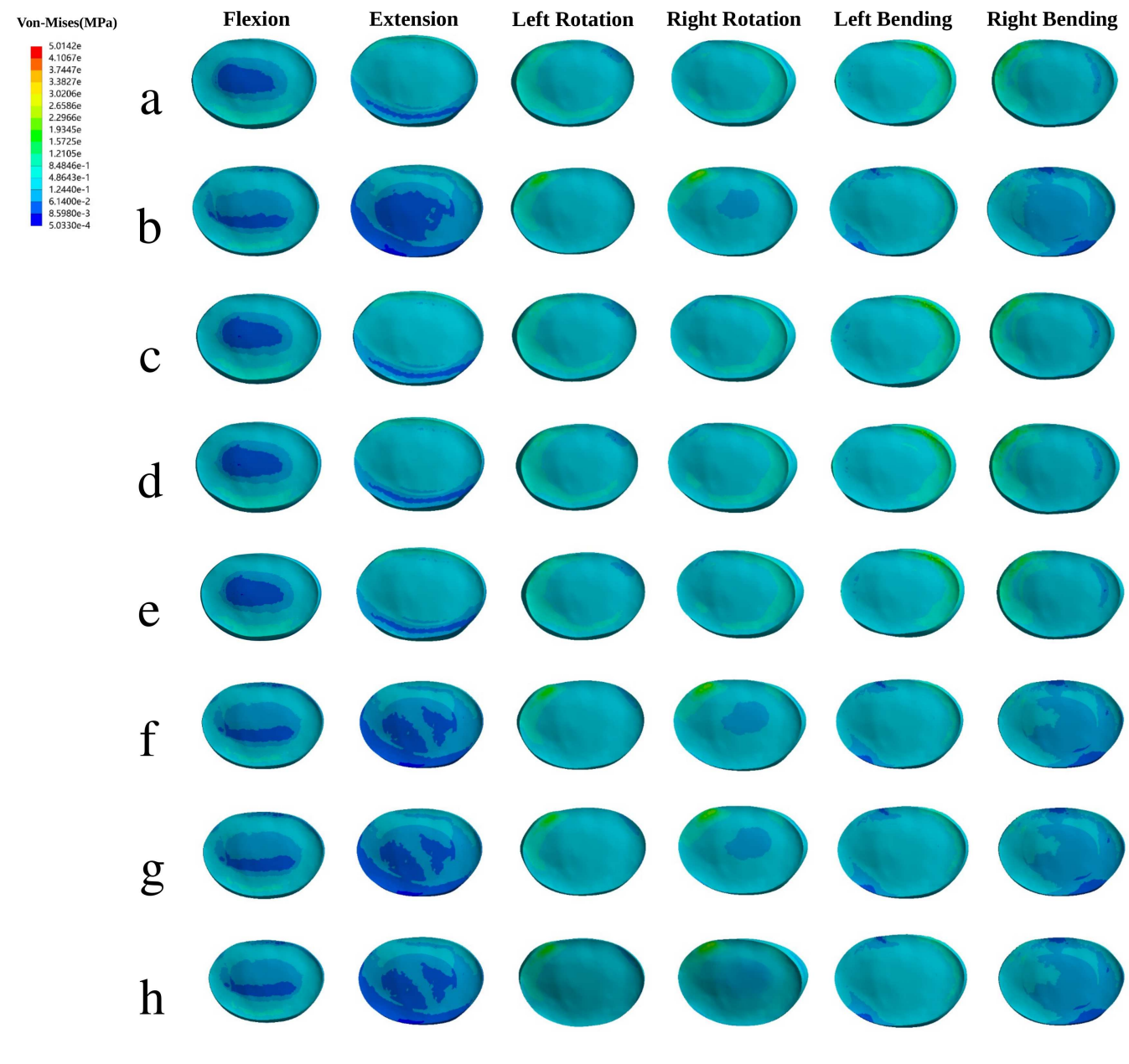

Von-Mises(MPa)
3.5221e1
3.2113e1
2.9006e1
2.5898e1
2.2790e1
1.9683e1
1.6575e1
1.3467e1
1.0360e1
7.9450e
5.6488e
3.8434e
1.6759e
8.6410e-1
6.9750e-2
7.6741e-3
Flexion
Extension
Left Rotation
Right Rotation
Left Bending
Right Bending
a
b
c
d
e
f
g
h


Von-Mises(MPa)
5.6586e1
4.5117e1
3.6437e1
2.8149e1
2.1334e1
1.9472e1
1.7610e1
1.5748e1
1.3887e1
1.2025e1
1.0163e1
8.3011e
6.4392e
4.5774e
2.4760e
0.0000e
Flexion
Extension
Left Rotation
Right Rotation
Left Bending
Right Bending
a
b
c
d
e
f
g
h


MC type I
MC type II
MC type III
Isolated MC
Disc degeneration + MC
(a) L4 MC-region margin: maximum stress
(b) L4 MC-region margin: mean stress
(c) L5 MC-region margin: maximum stress
(d) L5 MC-region margin: mean stress
von Mises stress (MPa)
Flexion
Extension
Left rotation
Right rotation
Left bending
Right bending


a. Disc degeneration vs normal
b. MC I vs normal
c. MC II vs normal
d. MC III vs normal
e. DD + MC I vs normal
f. DD + MC II vs normal
g. DD + MC III vs normal
Flexion
Extension
Left axial rotation
Right axial rotation
Left lateral bending
Right lateral bending
2
4
6
Model key
Normal
Disc degeneration
MC I
MC II
MC III
DD + MC I
DD + MC II
DD + MC III
Segmental range of motion (degrees)


a Segmental ROM
DD vs normal
MC I vs normal
MC II vs normal
MC III vs normal
DD + MC I vs DD
DD + MC II vs DD
DD + MC III vs DD
-17.7 -83.6 -40.6 -44.4 -69.4 -78.3
-7.3 -0.5 -4.7 -2.0 -3.8 -5.8
-7.3 -0.5 -4.7 -2.0 -4.0 -6.0
-7.7 -0.8 -4.7 -2.0 -4.2 -6.0
-9.3 3.2 -4.5 -2.1 -2.5 -2.0
-9.3 3.2 -4.5 -2.1 -2.5 -2.0
-9.8 3.2 -4.5 -2.1 -2.5 -3.1
Flex Ext L rot R rot L bend R bend
Loading condition
80 60 40 20 0 −20 −40 −60 −80
b Maximum disc stress
DD vs normal
MC I vs normal
MC II vs normal
MC III vs normal
DD + MC I vs DD
DD + MC II vs DD
DD + MC III vs DD
-25.6 -69.2 -5.5 39.6 -67.5 -73.2
45.5 11.1 0.0 14.3 7.0 -6.3
43.0 11.1 0.0 14.3 7.0 -6.3
22.3 11.1 0.0 14.3 7.0 -6.5
-4.4 12.5 -3.4 -2.0 7.4 15.9
-4.4 12.5 -3.4 -2.0 6.7 15.9
-4.4 12.5 -3.4 -2.0 6.7 15.2
Flex Ext L rot R rot L bend R bend
Loading condition
40 20 0 −20 −40
Color scale: relative change (%)


Von-Mises(MPa)
5.0142e
4.1067e
3.7447e
3.3827e
3.0206e
2.6586e
2.2966e
1.9345e
1.5725e
1.2105e
8.4846e-1
4.8643e-1
1.2440e-1
6.1400e-2
8.5980e-3
5.0330e-4
Flexion
Extension
Left Rotation
Right Rotation
Left Bending
Right Bending
a
b
c
d
e
f
g
h

Supplementary Files

This is a list of supplementary files associated with this preprint. Click to download.

- Additionalfile1.docx
- Additionalfile2.csv
- Additionalfile3.csv